Allergy

WILEY

Allergy EUROPEAN JOURNAL OF ALLERGY AND CLINICAL IMMUNOLOGY EAACI

ORIGINAL ARTICLE OPEN ACCESS

Drug Allergy, Insect Sting Allergy, and Anaphylaxis

Targeting the Galectin-7/TRPM2/Zn^{2+}/DRP-1 Signaling Pathway: A Potential Therapeutic Intervention in the Pathogenesis of SJS/TEN

Chen Zhang[1] | BingYu Pang[1] | YiXin Luo[1] | Zipeng Cao[2] | Pei Qiao[1] | ZhenLai Zhu[1] | Hui Fang[1] | JianKang Yang[1] | ErLe Dang[1] | ShengXian Shen[1] | Pan Kang[1] | Qingqing Jiao[3] | Akito Hasegawa[4] | Riichiro Abe[4] | HongJiang Qiao[1] | Gang Wang[1] | Meng Fu[1]

[1]Department of Dermatology, Xijing Hospital, Fourth Military Medical University, Xi'an, China | [2]Department of Health Education and Management and the Ministry of Education Key Lab of Hazard Assessment and Control in Special Operational Environment, School of Public Health, Fourth Military Medical University, Xi'an, China | [3]Department.of Dermatology, The First Affiliated Hospital of Soochow University Central Research Laboratory, Suzhou, China | [4]Division of Dermatology, Niigata University Graduate School of Medical and Dental Sciences, Niigata, Japan

Correspondence: Riichiro Abe (aberi@med.niigata-u.ac.jp) | HongJiang Qiao (xjhongjiangq@fmmu.edu.cn) | Gang Wang (wanggangxjyy@163.com) | Meng Fu (2239874942@qq.com)

Received: 24 June 2024 | **Revised:** 26 December 2024 | **Accepted:** 15 January 2025

Funding: This study was supported by the National Natural Science Foundation of China (Grant Nos. 82373472 (C.Z.) and 82173409 (M.F.)) and the Xijing Hospital Innovative and Special Medical Research Project (XJZT24CY32 (C.Z.) and XJZT24JC26 (M.F.)).

Keywords: apoptosis | exosomes | galectin-7 | mitochondria | mitochondrial fission | Stevens–Johnson syndrome | toxic epidermal necrolysis | TRPM2 | Zn^{2+}

ABSTRACT

Background: Stevens–Johnson syndrome (SJS) and toxic epidermal necrolysis (TEN) represent a spectrum of severe drug-induced cutaneous reactions. These conditions are characterized by widespread and confluent keratinocyte apoptosis, which differentiates them from erythema multiforme (EM). Mounting evidence has implicated the mitochondrial-dependent apoptosis pathway in the pathogenesis of SJS/TEN, but the potential roles and specific mechanisms of these pathways in SJS/TEN remain largely unexplored.

Methods: Proteomic analyses were conducted to investigate differential protein expression in blister fluid (BF)-derived exosomes from suction surgery in healthy individuals (Con Exo) or patients with EM (EM Exo) or SJS/TEN (TEN Exo). Further analysis involved glutathione S-transferase (GST) pull-down assay, liquid chromatography–tandem mass spectrometry (LC–MS/MS) analysis, and validation of MS results through proximity ligation assay (PLA) and coimmunoprecipitation (co-IP). Phenotypic and mechanistic analyses were performed using immunohistochemistry (IHC) staining, enzyme-linked immunosorbent assay (ELISA), western blotting, reverse transcription–polymerase chain reaction (RT-PCR), co-IP, CCK-8 assay, adenosine triphosphate (ATP) level measurements, and flow cytometry.

Results: Galectin-7 was markedly upregulated in BF-derived exosomes from SJS/TEN patients and showed a correlation with disease severity. Further analysis confirmed the interaction between galectin-7 and transient receptor potential (melastatin) 2 (TRPM2). BF-derived exosomes from SJS/TEN patients induced an imbalance in mitochondrial dynamics via galectin-7/TRPM2

Abbreviations: DRP-1, Dynamin-related protein-1; ETCx, Electron transport chain complexes; Hessian-SIM, Hessian-structured illumination microscopy; HK2, Hexokinase 2; Mdivi-1, Mitochondrial division inhibitor-1; MMP, Mitochondrial membrane potential; mPTP, Mitochondrial permeability transition pore; SCORTEN, A severity-of-illness score for toxic epidermal necrolysis; SJS, Stevens–Johnson syndrome; TEN, Toxic epidermal necrolysis; TRPM2, Transient receptor potential channel, subtype melastatin 2; VDAC1, Voltage-dependent anion channel 1.

Chen Zhang, BingYu Pang, YiXin Luo, Zipeng Cao and Pei Qiao authors contributed equally to this study.

upregulation. Activation of TRPM2 led to an elevation in mitochondrial Zn^{2+}, which facilitated the recruitment of the fission factor dynamin-related protein-1 (DRP-1) to mitochondria to trigger mitochondrial fission in the keratinocyte. In addition, the recruitment of DRP-1-dependent mitochondrial fission via the voltage-dependent anion channel 1 (VDAC1)/hexokinase 2 (HK2)-mediated opening of the mitochondrial permeability transition pore (mPTP)-triggered cytochrome c release. These effects ultimately induce activation of the intrinsic mitochondrial apoptotic pathway and contribute to the pathogenesis of SJS/TEN.
Conclusions: Targeting the galectin-7/TRPM2/Zn^{2+}/DRP-1 signaling pathway in keratinocytes presents a prospective therapeutic strategy for mitigating SJS/TEN in the future.

1 | Introduction

Stevens–Johnson syndrome (SJS) and toxic epidermal necrolysis (TEN) are rare, acute, and life-threatening mucocutaneous diseases that are nearly always drug-related [1, 2]. They are a consequence of extensive keratinocyte apoptosis that results in the separation of significant areas of skin at the dermal–epidermal junction, producing the appearance of scalded skin. Considered as part of the same spectrum of diseases, SJS has skin detachment on less than 10% of the body surface area (BSA), whereas TEN is defined as the area of denuded skin greater than 30% of BSA; the range of 10%–30% is known as SJS-TEN overlap.

To date, the mechanism of keratinocyte apoptosis in SJS/TEN is not fully understood. Previous studies have shown that certain pathogenic factors, including the extrinsic apoptosis pathway: Fas–Fas ligand (FasL) interactions and TNF-α; granule exocytosis pathway: perforin/granzyme and granulysin, play an important role in triggering apoptosis of keratinocytes in SJS/TEN [3, 4]. Recent research also implicates intrinsic apoptosis as an alternate pathway in mediating keratinocyte cell death in SJS/TEN [5, 6]. In mice, subcutaneous injection of a small molecule inhibitor of apoptosis (IAP) antagonist drug (smac-mimetic, SM) induced TEN-like cutaneous inflammation, epidermal detachment, and histological features of TEN [7]. Our group has shown that the intrinsic pathway is activated by plasma exosomal *miR-375-3p* via downregulation of the X-linked inhibitor of apoptosis protein (XIAP), leading to mPTP opening, which initiates a signaling cascade that leads to cell death [6].

During apoptosis, one of the steps is the fragmentation of mitochondria, and recent evidence indicates that mitochondrial fission is critical for apoptotic promotion [8, 9]. In particular, DRP-1 mediates mitochondrial fission, leading to mPTP opening, cytochrome c release, and subsequently initiates mitochondrial-dependent cellular apoptosis [10]. In our previous study, a shift of mitochondrial dynamics towards fission has been observed in SJS/TEN lesions [6]. Since mitochondrial homeostasis is an essential housekeeping function to maintain cell viability and excessive mitochondrial fission provokes apoptosis [11], we hypothesized that aberrant mitochondrial fission may also influence the execution of keratinocyte apoptosis in SJS/TEN. However, the mechanisms regarding regulating their aberrant mitochondrial fission and the subsequent apoptosis process are still insufficiently understood.

For assessment of mitochondrial fission and apoptosis mechanisms, here we perform proteomic analysis of BF-derived exosomes from SJS/TEN patients, EM patients, and suction surgery blisters from healthy individual groups. We identified galectin-7 as a candidate molecule for driving mitochondrial fission and the subsequent apoptosis process. Importantly, the TRPM2 channel in keratinocytes was activated by galectin-7 from BF-derived exosomes from SJS/TEN patients, which altered intracellular Zn^{2+} homeostasis, leading to aberrant recruitment of DRP-1 and excessive mitochondrial fission. These findings raise the exciting perspective of targeting the galectin-7/TRPM2/Zn^{2+}/DRP-1 pathway as a novel therapeutic strategy to treat SJS/TEN.

2 | Results

2.1 | Characterization of BF-Derived Exosomes From SJS/TEN Patients

Patients with SJS/TEN exhibit multiple erythematous macules evolving into bullae and epidermal detachment on the limbs (Figure 1A). The histopathology of SJS/TEN is characterized by a subepidermal cleft with overlying confluent necrosis of the epidermis (Figure 1B). SJS/TEN BF was an immune-rich reservoir devoid of stromal subsets [12], and exosomes participate in the development of allergic diseases [13, 14]. Therefore, the exosome-rich fraction was purified from BF of SJS/TEN patients with a standard protocol of ultracentrifugation steps (Figure 1C). Using transmission electron microscopy (TEM), we observed the typical 'cup-shaped' vesicles of exosomes ~100 nm in diameter (Figure 1D). Western blotting analysis indicated that the exosomes were positive for the CD9, CD63, TSG101, and CD81 markers (Figure 1E). The average particle sizes lay within the expected 30–200 nm range by Nano-Flow Cytometry (NanoFCM) (Figure 1F). Subsequently, the specific antibody captured on each ExoView chip spot was used for antibody capture-based immobilization of exosome samples for further probing with fluorescently labeled antibodies (Figure 1G). Single particle interferometric reflectance imaging sensing (SP-IRIS) analysis indicated that the sizes of the Con Exo and TEN Exo were similar (Figure 1H). Immuno-colocalization imaging indicated that TEN Exo had more CD9-, CD63-, and CD81-positive exosomes than the Con Exo ($p < 0.001$) (Figure 1I,J). Moreover, the higher percentages of $CD81^+/CD9^+$, $CD63^+/CD81,^+$ and $CD63^+/CD81^+/CD9^+$ cells in the TEN-Exo group compared with those in the Con-Exo group ($p < 0.05$) (Figure 1K,L). Interestingly, greater numbers of monocyte-derived $CD14^+/CD63^+$, Natural killer (NK) cell-derived $CD56^+/CD63^+$, and cytotoxic T-cell-derived $CD8^+/CD63^+$ exosomes were present in the TEN-Exo group ($p < 0.001$) (Figure 1M). These data showed that TEN Exo contained higher numbers of CD63-, CD81-, and CD9-positive nanoparticles.

We further investigated whether BF-derived exosomes from SJS patients (SJS Exo) and TEN patients (TEN Exo) have different pathogenic signatures regarding keratinocyte apoptosis.

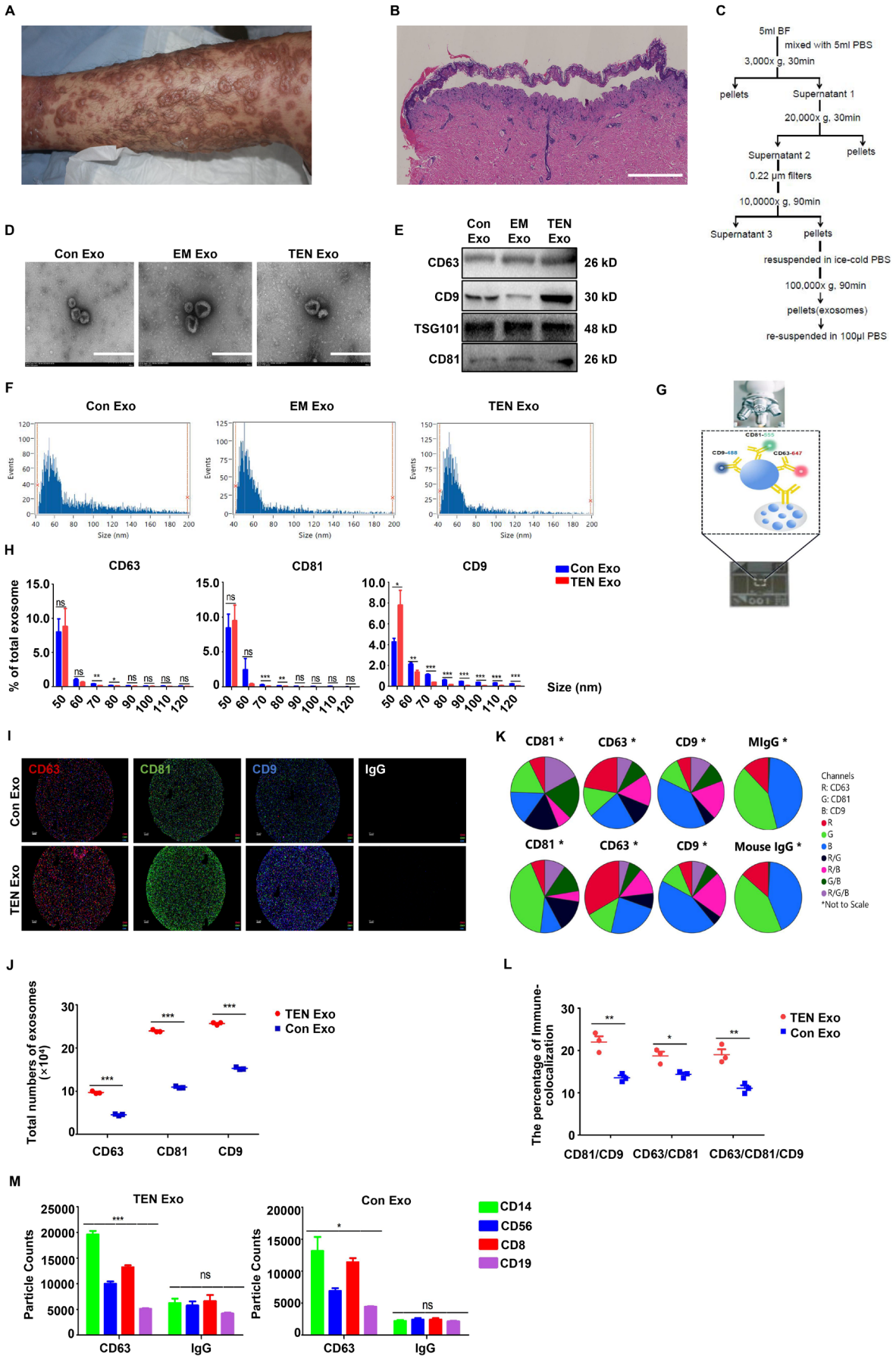

FIGURE 1 | Legend on next page.

FIGURE 1 | Characterization of BF-derived exosomes from SJS/TEN patients. (A) The blisters and erosions of patients with SJS/TEN. (B) Hematoxylin and eosin (H&E) staining shows the skin lesions of patients with SJS/TEN. (C) Flow chart for the exosome purification procedure based on differential ultracentrifugation. (D) Electron micrographs. (E) Western blotting analysis confirmed the presence of exosome marker proteins. (F) Size distribution of BF-derived exosomes determined using a Flow NanoAnalyzer. (G) Schematic diagram of the sensitive multimarker detection method for exosomes captured on a microarray chip. (H) The size distribution. (I, J) The number of exosome marker-captured subpopulations was analyzed by SP-IRIS analysis. (K, L) Immune-colocalization of the exosomes was determined by SP-IRIS. The chips were coated with antibodies against anti-human CD81, CD63, and CD9. Anti-mouse IgG was used as the negative control. Fluorescent antibodies against CD81, CD63, and CD9 were used for the analysis of colocalization. (M) Particle counts of captured $CD14^+$, $CD56^+$, $CD8^+$, and $CD19^+$ BF-derived exosomes from suction surgery in healthy individuals and SJS/TEN sample conditions on both CD63 and IgG capture spots. Con Exo, exosome obtained from suction surgery in healthy individuals; EM Exo, exosome from patients with EM; and TEN Exo, exosome from patients with SJS/TEN. *Bar* = 100 μm. The BF-derived exosomes were obtained from three patients with EM or SJS/TEN and three suction surgeries in healthy individuals, with each patient and suction surgery undergoing three biological replicates. ns, not significant. $^*p < 0.05$, $^{**}p < 0.01$, $^{***}p < 0.001$.

The results showed that both SJS Exo and TEN Exo can promote keratinocyte apoptosis. Specifically, SJS Exo dramatically downregulated cell viability and ATP levels, but upregulated intracellular reactive oxygen species (ROS) and caspase-3 activity in keratinocytes ($p < 0.01$) (Figure S1A–D). Importantly, TEN Exo significantly reduced human keratinocyte viability and ATP levels relative to SJS Exo (Figure S1A,B). Moreover, intracellular ROS and caspase-3 activity were upregulated in the TEN Exo group compared with the SJS Exo group ($p < 0.01$) (Figure S1C,D). In addition, TEN Exo also upregulated cleaved CAS-3, CAS-9, BAX, and poly (ADP-ribose) polymerase (PARP) but substantially downregulated BCL-2 compared to those with the SJS Exo group (Figure S1E). Together, these data suggest that TEN Exo promoted more apoptotic effects in keratinocytes relative to SJS Exo, but SJS Exo and TEN Exo have similar pathogenic signatures.

2.2 | Proteomic Analysis of BF-Derived Exosomes Obtained via Suction Surgery in Healthy Individuals or From Patients With EM and SJS/TEN

To elucidate the mechanisms underlying the apoptotic effect of BF-derived exosomes from SJS/TEN patients, we analyzed their protein content by mass spectrometry (MS). Proteomic analysis of differentially expressed proteins among Con Exo, EM Exo, and TEN Exo (The SCORTEN from No. 1–3 TEN patients were 1, 2, 3, respectively) was performed. The volcano plot in Figure 2A-C shows a total of 204 differentially expressed proteins (142 upregulated and 62 downregulated) between the TEN Exo and Con Exo groups based on a fold change > 2 and $p < 0.05$. Moreover, there were 22 upregulated proteins and 21 downregulated proteins in the TEN Exo group compared with the EM Exo group. Using WoLF PSORT software, the majority of the detected exosomal proteins were predicted to accumulate in the cytosol, extracellular space, and mitochondria (Figure 2D). Kyoto Encyclopedia of Genes and Genomes (KEGG) pathway annotation revealed that these differentially expressed proteins were related mainly to apoptosis and mitochondrial dynamics (Figure 2E). Notably, galectin-7 was the most prevalent protein found in TEN Exo in comparison to EM Exo and Con Exo. Thus, galectin-7 was selected for further examination in subsequent investigations.

2.3 | *Galectin-7*-siRNA-Exo-Fect Exosomes Suppress Keratinocyte Apoptosis In Vitro via a Mitochondrial-Dependent Pathway

We sought to investigate the potential involvement of galectin-7 in keratinocyte apoptosis in SJS/TEN patients. We first transfected human primary keratinocytes with *Galectin-7*-siRNA and validated the transfection efficiency by western blotting (Figure S2A). Notably, *Galectin-7*-siRNA–loaded TEN Exo (the SCORTEN from No. 2 and TEN patient was 2) significantly enhanced keratinocyte viability while reducing intracellular ROS and keratinocyte apoptosis levels ($p < 0.05$) (Figure S2B–E). The close link between mitochondrial abnormalities and apoptosis prompted an investigation into mitochondrial functions. The results showed that *Galectin-7*-siRNA–loaded TEN Exo hindered mitochondrial membrane potential (MMP) collapse, boosted ATP production, and lowered the adenosine diphosphate (ADP)/ATP ratio, and decreased the mitochondrial reactive oxygen species (mtROS) levels, collectively indicating mitochondrial dysfunction ($p < 0.05$) (Figure S2F–I). In addition, the delivery of *Galectin-7*-siRNA–loaded TEN Exo resulted in a reduction of BAX, BAK, cleaved CAS-3, CAS-9, and PARP levels while concurrently enhancing BCL-2 expression in keratinocytes (Figure S2J). Accordingly, galectin-7–loaded TEN Exo significantly reduced keratinocyte viability while increasing intracellular ROS levels and apoptosis ($p < 0.05$) (Figure S3A–E). In addition, galectin-7–loaded TEN Exo promoted MMP collapse, elevated the ADP/ATP ratio, and decreased ATP production (Figure S3F–H). Galectin-7–loaded TEN Exo also upregulated levels of BAX, BAK, cleaved CAS-3, CAS-9, and PARP, while downregulating BCL-2 levels in keratinocytes (Figure S3I).

In addition, we detected whether the other proteins in TEN Exo mediated the apoptotic effects of keratinocytes. The KEGG pathway annotation indicates that S100A9 and PDCD6 from TEN Exo may participate in the apoptosis pathway. However, *S100A9* or *PDCD6*-siRNA–loaded TEN Exo (the SCORTEN from No. 2 and TEN patient was 2) could not change keratinocyte viability, ATP level, caspase-3 activity, and the expression levels of apoptosis-related proteins compared with control-siRNA–loaded TEN Exo (Figure S4A–G). These data suggest that galectin-7 specifically facilitates keratinocyte apoptosis via a mitochondrial-dependent pathway.

FIGURE 2 | Legend on next page.

FIGURE 2 | Proteomic analysis of BF-derived exosomes obtained from suction surgery in healthy individuals and patients with EM or TEN. (A) Volcano plot of differentially expressed proteins among Con Exo, EM Exo, and TEN Exo. Each group consists of three patients, with each patient undergoing three biological replicates. (B, C) Heatmap and number of differentially expressed proteins among Con Exo, EM Exo, and TEN Exo. Each group consists of three patients, with each patient undergoing three biological replicates. (D, E) Subcellular location and KEGG pathway analysis of differentially expressed proteins among Con Exo, EM Exo, and TEN Exo.

2.4 | Identification of Galectin-7-Interacting Proteins by GST Pull-Down and LC–MS/MS Analysis

To further explore the specific molecules to which galectin-7 binds to promote keratinocyte apoptosis, we conducted a GST pull-down assay combined with LC–MS/MS to identify the proteins that interact with galectin-7. Purified GST and GST-galectin-7 proteins were subjected to SDS-PAGE and visualized by Coomassie brilliant blue staining. GST and GST-galectin-7 showed predominant bands at the expected molecular weight (Figure 3A). Among the 20 potential candidates, TRPM2 was distinguished by 2 unique peptides. Furthermore, the differentially expressed proteins were enriched mainly in the cell death pathway (Figure 3B–D). To verify this relationship, we performed rigid protein–protein docking between galectin-7 and TRPM2. As shown in Figure 3E, galectin-7 and TRPM2 form hydrogen bonds through amino acid residues such as ARG 134-GLN 433 and GLN 129-SER 421, revealing that the galectin-7 and TRPM2 proteins form a stable protein docking model. The conformation of the ligand–protein complex also suggested that galectin-7 is stably bound to the TRPM2 protein at the active site, as determined by root-mean-square deviation (RMSD) analysis (Figure 3F). To corroborate these results and to confirm the interaction between galectin-7 and TRPM2, a duolink PLA was performed with keratinocyte and transfected with *Galectin-7*-siRNA or a negative control. As shown in Figure 3G, red fluorescence was found in the cytoplasm of the keratinocyte, which displayed hybridized and amplified antibody-linked nucleotide strands revealing the interaction between galectin-7 and TRPM2. Moreover, the relative fluorescence intensity of PLA was decreased after transfection with *Galectin-7*-siRNA. We also demonstrated that the galectin-7 and TRPM2 complex was stably associated in HaCaT cells, and these interactions were activated mainly in mitochondria (Figure 3H).

2.5 | Skin Lesions and BF or BF-Derived Exosomes From SJS/TEN Patients Show Increased Levels of Galectin-7 and TRPM2

In order to clarify whether galectin-7 and TRPM2 could participate in the pathogenesis of SJS/TEN, we then explored the expression of galectin-7 and TRPM2 in vivo. First, IHC and western blotting revealed that the levels of galectin-7 and TRPM2 were significantly increased in the epidermis of SJS/TEN lesions (The SCORTEN from No. 1–3 TEN patients were 1, 2, 3, respectively; The SCORTEN from No. 5 SJS patient was 2) compared with those of patients with EM or maculopapular drug eruption (MPE) and healthy individuals (Figure 4A,B). Interestingly, we found that the expression levels of galectin-7 and TRPM2 in the epidermis of TEN patients were clearly higher compared to patients with psoriasis and atopic dermatitis (AD) (Figure 4C). Moreover, galectin-7 and TRPM2 expression in the epidermis of TEN patients was significantly reduced after system corticosteroids (Figure 4D) or TNF inhibitor Etanercept treatment ($p < 0.01$) (Figure S5A,B). TRPM1 was also a member of the family of melastatin-related TRPM channels. To further elucidate whether TRPM1 could be involved in the pathogenesis of SJS/TEN, we detected the expression level of TRPM1 in vivo. The results showed that TRPM1 expression was not changed in SJS/TEN patients relative to EM, MPE patients, and healthy individuals, as indicated in Figure S5C,D. In addition, the BF-derived exosomes and BF from SJS/TEN patients presented obviously higher galectin-7 levels than those from patients with EM and those obtained via suction surgery in healthy individuals ($p < 0.01$) (Figure S5E,F). We also observed that galectin-7 levels in TEN Exo were higher relative to SJS Exo ($p < 0.05$) (Figure S5G). Moreover, these levels were positively correlated with the disease severity of BSA and the severity-of-illness score for toxic epidermal necrolysis (SCORTEN) in SJS/TEN patients (Figure S5H–K). These data indicated that galectin-7 and TRPM2 may be associated with the pathological mechanisms of SJS/TEN.

2.6 | TRPM2 Promotes Keratinocyte Apoptosis In Vitro via a Mitochondrial-Dependent Pathway

To prove whether TRPM2 could mediate the apoptotic effect of keratinocytes in vitro, we first transfected human primary keratinocytes with *TRPM2*-siRNA or negative control siRNA and confirmed the transfection efficiency by western blotting (Figure S6A). Notably, *TRPM2*-siRNA or an inhibitor (clotrimazole) significantly increased keratinocyte viability and decreased intracellular ROS levels (Figure S6B–D). *TRPM2*-siRNA or an inhibitor decreased the ADP/ATP ratio and keratinocyte apoptosis, and hindered MMP collapse ($p < 0.05$) (Figure S6E–G). In addition, *TRPM2*-siRNA or an inhibitor reduced the levels of BAX, BAK, cleaved-CAS-3, CAS-9, and PARP (Figure S6H). Moreover, compared with those from healthy individuals, the mitochondria from patients with TEN lacked cristae (Figure S6I).

To further elucidate whether TRPM2 inhibition can attenuate the apoptotic effects mediated by galectin-7 on keratinocytes, we transfected galectin-7 plasmid-pretreated TEN Exo with *TRPM2-siRNA* or TRPM2 inhibitor. Notably, *TRPM2-siRNA* or an inhibitor significantly upregulated keratinocyte viability and ATP levels, dramatically decreased intracellular ROS levels, caspase-3 activity, and the expression levels of BAX, BAK, cleaved-CAS-3, CAS-9, and PARP from galectin-7-mediated apoptotic effects on keratinocytes ($p < 0.05$) (Figure S7A–E). Therefore, TRPM2 inhibition can attenuate the apoptotic effects mediated by galectin-7 on keratinocytes. These results demonstrated that exosomal galectin-7 entered into keratinocytes, combined with TRPM2, and induced keratinocyte apoptosis via a mitochondrial-dependent pathway.

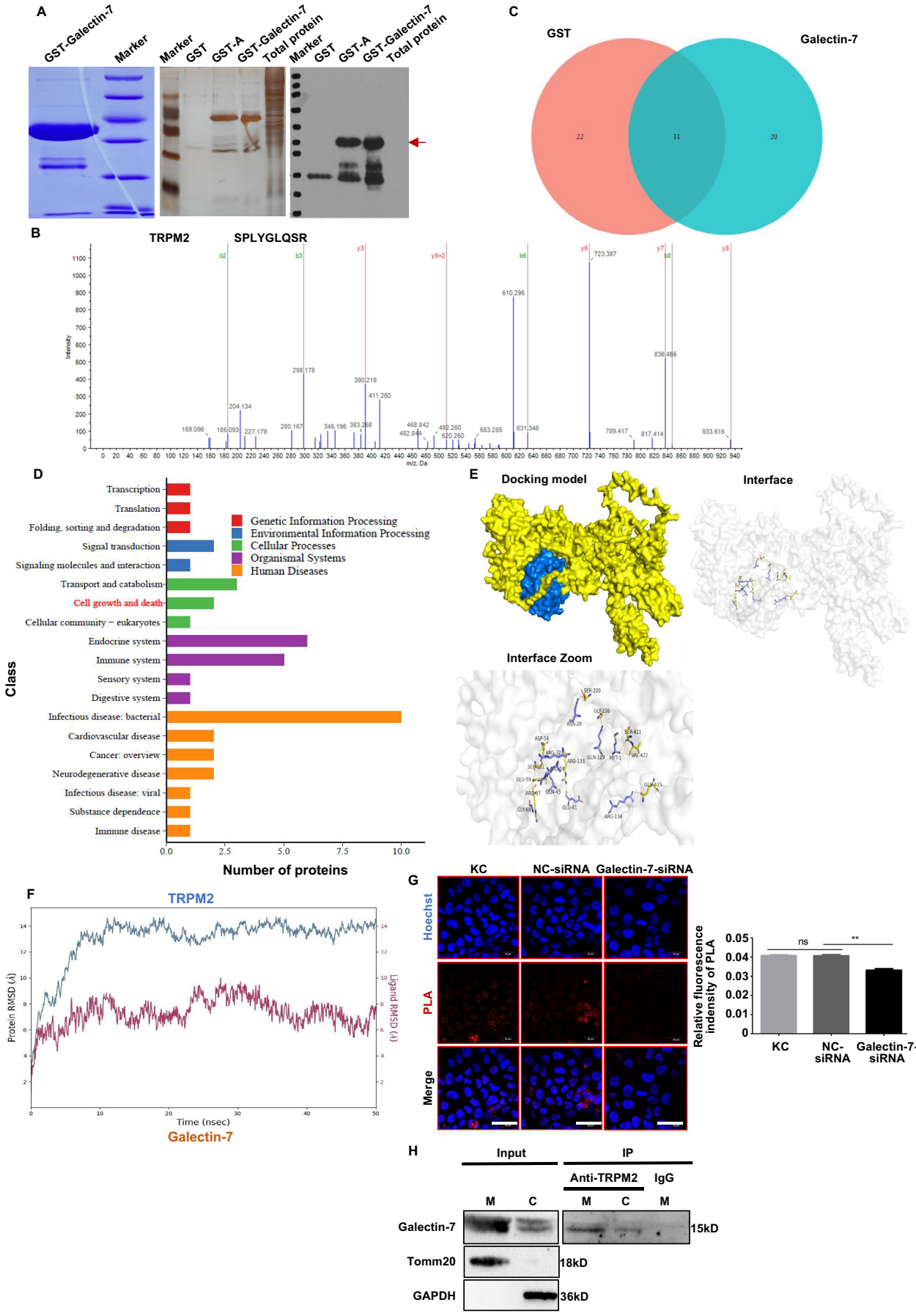

FIGURE 3 | Legend on next page.

FIGURE 3 | Galectin-7 forms a stable complex with the TRPM2 protein. (A) SDS-PAGE and western blotting results show several proteins identified by large-scale GST pulldown. (B) The differential bands were analyzed by LC–MS/MS. (C) Venn diagram of the GST and galectin-7-related proteins. (D) Enrichment pathway analysis of galectin-7-related differentially expressed proteins. (E) Surface diagram of the docking model and residues of galectin-7 that interact with the TRPM2 protein (galectin-7, blue; TRPM2, yellow; hydrogen bond interaction, dotted line). (F) Molecular dynamics analysis of ligand–receptor complexes. The RMSD reflects the stability of the galectin-7/TRPM2 complex. (G) The duolink PLA was used to detect the colocalization and interaction between galectin-7 and TRPM2. *Bar* = 50 μm. (H) co-IP analysis showed the reciprocal binding of galectin-7 and TRPM2 in HaCaT cells. C, Cytoplasm; M, Mitochondria; ns, not significant. $^{**}p < 0.01$.

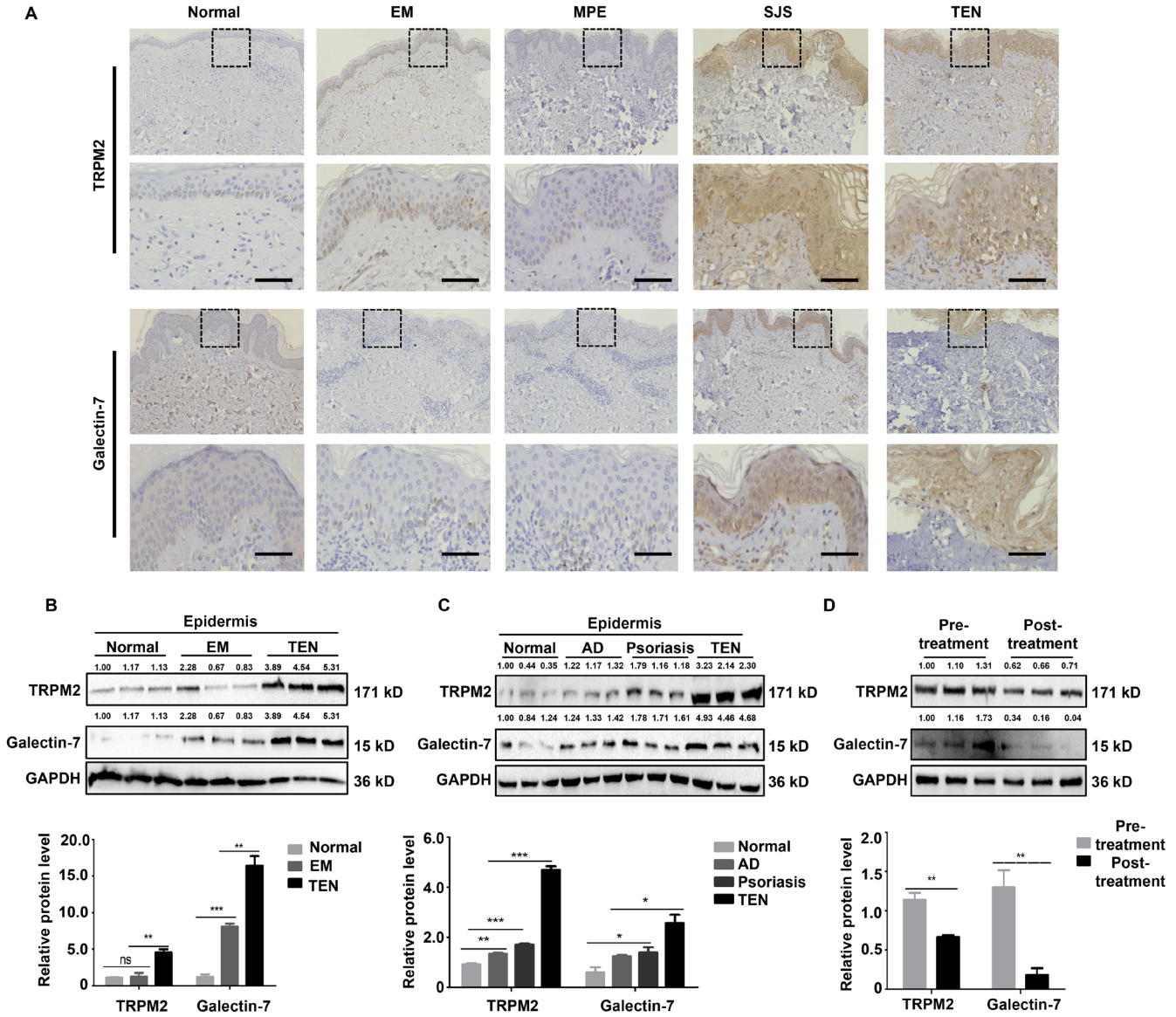

FIGURE 4 | Galectin-7 and TRPM2 protein expression in vivo. (A) Galectin-7 and TRPM2 immunostaining. *Bar* = 100 μm. (B) Western blotting showing the expression of galectin-7 and TRPM2 in the epidermis of skin biopsy samples from healthy individuals and patients with EM or TEN. (C) Western blotting showing the expression of galectin-7 and TRPM2 in the epidermis of skin biopsy samples from healthy individuals and patients with AD, psoriasis, or TEN. Densitometry was used to measure the expression levels of galectin-7 and TRPM2 relative to those of GAPDH. (D) Galectin-7 and TRPM2 expression in the epidermis of TEN patients before and after treatment with system corticosteroids. The data are representative of at least three independent experiments. ns, not significant. $^{*}p < 0.05$, $^{**}p < 0.01$, $^{***}p < 0.001$.

2.7 | Galectin-7/TRPM2 Contributes to Disruption of the Mitochondrial Structure and Function

In order to determine how galectin-7 and TRPM2 induce keratinocyte apoptosis, we focused on changes in the mitochondrial structure and function. First, we revealed that the mitochondrial DNA (mtDNA) copy number and transcripts were decreased after treatment with TEN Exo, but treatment with *TRPM2*- or *Galectin*-7-siRNA–loaded TEN Exo reversed these changes (Figure 5A). The electron transport chain complex (ETCx) is

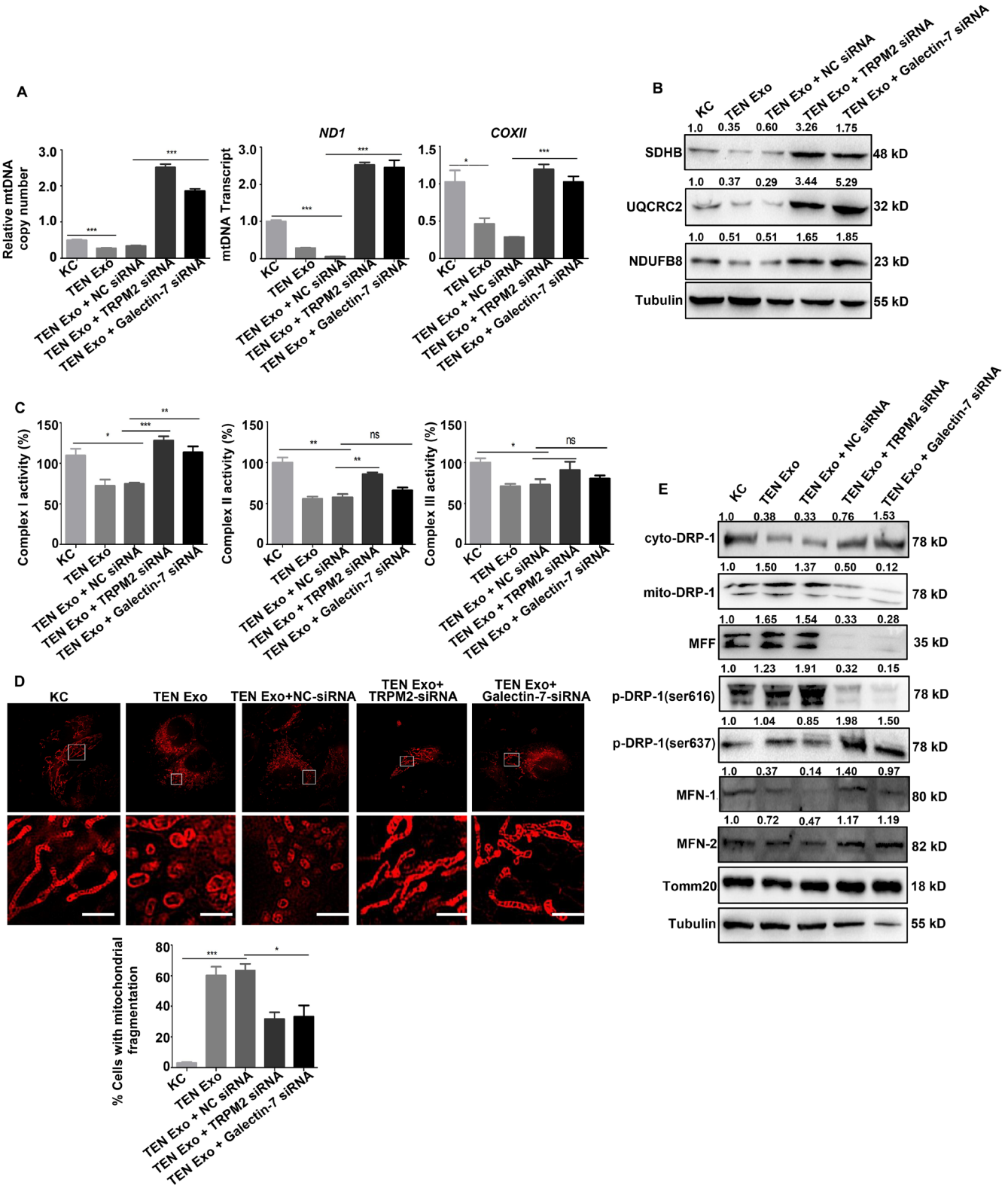

FIGURE 5 | Galectin-7 or TRPM2 siRNA protects mitochondrial function in keratinocytes. (A–E) Human primary keratinocytes were incubated with *Galectin-7* or *TRPM2*-siRNA–loaded TEN Exo for 48 h. (A) qRT-PCR analyses of the mtDNA copy number. The transcript level of mtDNA is reflected by two different components: ND1, encoded by the light chain of mtDNA, and COX II, encoded by the heavy chain of mtDNA. (B) Protein expression of the mitochondrial ETCx. (C) The changes in ETCx I, II, and III activities were measured spectrophotometrically. (D) HIS-SIM recording of the mitochondrial morphology and cristae of human primary keratinocytes labeled with PKMO. *Bar* = 100 μm. (E) The protein expression levels of DRP-1, MFF, MFN-2, and MFN-1 were analyzed via western blotting. The data are representative of at least three independent experiments. ns, not significant. $^{*}p < 0.05$, $^{**}p < 0.01$, $^{***}p < 0.001$.

encoded mainly by mtDNA. TEN Exo reduced the content and function of ETCx, but *TRPM2*- or *Galectin-7*-siRNA–loaded TEN Exo increased the content and function of ETCx (Figure 5B,C). In parallel, compared with TEN Exo treatment, TRPM2 or galectin-7–loaded TEN Exo treatment further decreased the mtDNA copy number, ETCx content, and mitochondrial biogenesis ($p < 0.05$) (Figure S8A–D).

Imbalanced mitochondrial dynamics are associated with a range of diseases that are broadly characterized by impaired mitochondrial function and increased cell death [15]. The efficiency of mitochondrial respiration and cellular growth depends on the cristae shape [16]. Therefore, we stained human primary keratinocytes using PK Mito Orange (PKMO) and captured individual mitochondrial cristae. Hessian-structured illumination microscopy (HIS-SIM) revealed that mitochondria in a normal keratinocyte exhibited a highly ordered lamellar crista architecture across the entire mitochondrial network and a long tubular, branched mitochondrial network (Figure 5D). In contrast, treatment with TEN Exo led to significant fragmentation of the network into small rounded fragments in the majority of cells, and the crista arrangements appeared to be less regular or lacked cristae (Figure 5D); however, *TRPM2*- or *Galectin-7*-siRNA–loaded TEN Exo reversed these changes (Figure 5D).

Mitochondrial fission is induced by the translocation of DRP-1 from the cytosol to the mitochondria [10]. Our results showed that TEN Exo significantly promoted and inhibited the overlap among DRP-1, cytochrome c, and mitochondria compared with that obtained with the control treatment. However, in the *TRPM2*- or *Galectin-7*-siRNA–loaded TEN Exo groups, the number of DRP-1 or cytochrome c foci on the mitochondria was clearly decreased or increased, respectively, as revealed by immunofluorescence analysis and western blotting (Figure S9A,B). Phosphorylation at serine 616 (DRP-1 S616) is associated with increased DRP-1 activity (pro-fission), whereas phosphorylation at serine 637 (DRP-1 S637) has the opposite effect (antifission) [10]. The data showed that TEN-Exo treatment increased the phosphorylation of DRP-1 at ser616 and decreased that at ser637 (Figure 5E). However, these changes were reversed by treatment with *TRPM2*- or *Galectin-7*-siRNA–loaded TEN Exo (Figure 5E). In addition, we found that TRPM2 and galectin-7 strongly reduced the expression of proteins related to mitochondrial fusion, including mitofusin 1 (MFN1) and mitofusin 2 (MFN2) (Figure 5E). Furthermore, IHC revealed that the expression of the mitochondrial electron transfer chain such as NADH dehydrogenase [ubiquinone] 1 beta subcomplex subunit 8 (NDUFB8), succinate dehydrogenase enzyme B (SDHB), ubiquinol-cytochrome c reductase core protein 2 (UQCRC2); mitochondrial biogenesis biomarkers such as PPAR-gamma coactivator 1alpha (PGC-1α), nuclear respiratory factor 1 (NRF1), mitochondrial transcription factor A (TFAM), and MFN-2 were downregulated in the skin lesions of SJS/TEN patients compared with those of patients with EM or MPE and healthy individuals. In contrast, the expression of DRP-1 and mitochondrial fission factor (MFF) were upregulated in the skin lesions of SJS/TEN patients compared with those of patients with EM or MPE and healthy individuals (Figures S10–S12). Taken together, these data demonstrated that TEN Exo induced an imbalance in mitochondrial dynamics, leading to excessive mitochondrial fission via galectin-7/TRPM2 upregulation and subsequent DRP-1 recruitment to mitochondria.

2.8 | TRPM2 Induces an Increase in the Zn^{2+} Level in Mitochondria

Studies have shown that TRPM2 activation increases the cytosolic Ca^{2+} and Zn^{2+} levels [17]. Accordingly, we treated HaCaT cells with a TRPM2 plasmid and isolated mitochondria. Inductively coupled plasma mass spectrometry (ICP–MS) showed that the Zn^{2+} level in mitochondria was higher than the other ion levels (Figure 6A). The levels of serum Zn^{2+} were also significantly higher in SJS/TEN patients than in patients with EM and healthy individuals ($p < 0.01$) (Figure 6B). Intriguingly, the Zn^{2+} concentration in mitochondria was lower in the *TRPM2*-siRNA–loaded TEN-Exo groups than in the control group (Figure 6C).

Because mitochondria can sequester free Zn^{2+}, mitochondrial fission was prevented by Zn^{2+} chelation [18], and we speculated that there would be changes in the mitochondrial Zn^{2+} concentration in SJS/TEN keratinocytes. To test this hypothesis, we examined the effect of TEN Exo on the mitochondrial Zn^{2+} distribution by staining HaCaT cells with PK-Zinc and MitoTracker Red to label Zn^{2+} (green) and mitochondria (red), respectively. The presence of numerous yellow puncta in the merged images of TEN Exo-treated cells indicated the presence of Zn^{2+} in fragmented mitochondria (Figure 6D,E). We next examined the role of TRPM2 in the TEN Exo-induced increase in the mitochondrial Zn^{2+} concentration. The data suggested that *TRPM2* siRNA inhibited the redistribution of Zn^{2+} to mitochondria (Figure 6D,E). These results indicate that the TRPM2 channel-mediated mitochondrial Zn^{2+} increase.

2.9 | The Galectin-7/TRPM2 Complex Induces Mitochondrial Fission, Apoptosis, and DRP-1 Recruitment to Mitochondria Through Modulating Zn^{2+} Dynamics

Previous studies have shown that N,N,N′,N′-tetrakis (2-pyridylmethyl) ethylenediamine (TPEN), a specific Zn^{2+}-chelating agent, effectively suppresses the escalation of neuronal cell death [19]. Based on the aforementioned results, we examined the role of Zn^{2+} in TEN Exo-induced keratinocyte apoptosis. Our findings showed that TPEN markedly decreased keratinocyte apoptosis, intracellular ROS levels, and the ADP/ATP ratio while enhancing keratinocyte viability and MMP collapse following TEN Exo treatment. Conversely, elevating cytosolic Zn^{2+} levels with the Zn^{2+}-specific ionophore pyrithione (Zn-PTO) significantly augmented keratinocyte apoptosis, intracellular ROS levels, and the ADP/ATP ratio, while diminishing keratinocyte viability and MMP collapse ($p < 0.05$) (Figure 7A–E). Furthermore, TPEN decreased the levels of BAX, BAK, cleaved-CAS-3, CAS-9, and upregulated BCL-2 expression in keratinocytes, and Zn-PTO reversed these changes (Figure S13A).

An increase in mitochondrial Zn^{2+} triggers mitochondrial fragmentation [20]. Our findings indicated that TPEN treatment decreased the phosphorylation of DRP-1 at Ser616 and on mito-DRP-1, while increasing phosphorylation at Ser637 and

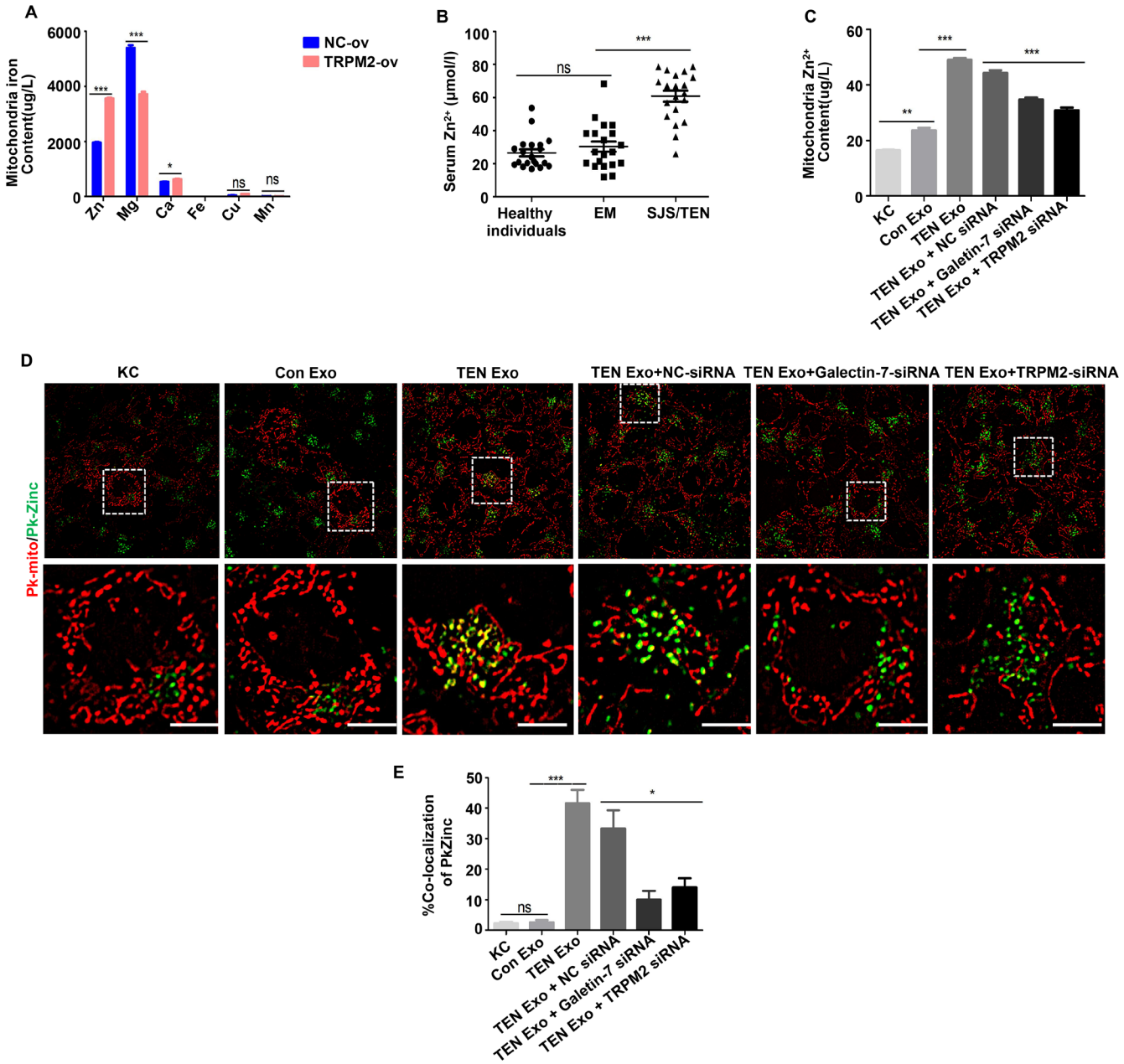

FIGURE 6 | TEN Exo increases the mitochondrial Zn^{2+} levels through galectin-7/TRPM2 complex activation. (A) Iron levels in mitochondria from HaCaT cells treated with the negative control or TRPM2 plasmid ($n = 3$). (B) Serum Zn^{2+} levels in healthy individuals and patients with EM or SJS/TEN ($n = 20$). (C) Zn^{2+} levels in mitochondria from HaCaT cells treated with Con Exo (100 ng/mL), TEN Exo (100 ng/mL), or *Galectin-7* and *TRPM2*-siRNA–loaded TEN Exo ($n = 3$). (D) Fluorescence images of HaCaT cells costained for Zn^{2+} (PK-Zinc) and mitochondria (PKMO). Images were taken after 48 h of exposure to TEN Exo or *Galectin-7* and *TRPM2*-siRNA–loaded TEN Exo. The boxed regions in the merged images are magnified in the underneath panels. *Bar* = 200 μm. (E) The percentage of PK-Zinc colocalization with PKMO was calculated from the data in D; the data are represented as the mean ± SEMs ($n = 3$). ns, not significant. $^{*}p < 0.05$, $^{**}p < 0.01$, $^{***}p < 0.001$.

on cyto-DRP-1 (Figure S13B). HIS-SIM and TEM revealed that TPEN-treated keratinocytes exhibited a well-organized lamellar crista architecture across their mitochondrial network, characterized by elongated tubular branches. In contrast, Zn-PTO–treated keratinocytes exhibited irregular or absent cristae, leading to the fragmentation of mitochondria into small, rounded shapes in most cells (Figure 7F,H).

Mitochondrial fragmentation is initiated by the recruitment of DRP-1 [9]. Our hypothesis posits that the elevation of mitochondrial Zn^{2+} levels, dependent on TRPM2, triggers the recruitment of DRP-1. To test this hypothesis, we transfected HaCaT cells with DRP-1 green fluorescent protein (GFP) and monitored its recruitment from the cytoplasm to the mitochondria. TEN Exo promoted DRP-1 mitochondrial recruitment, as assessed by the colocalization of MitoTracker Red fluorescence with that of DRP-1-GFP (Figure 7G and Figure S14). *Galectin-7*/*TRPM2*-siRNA suppressed the recruitment of DRP-1-GFP in response to TEN-Exo treatment (Figure S14). These results demonstrated that galectin-7/TRPM2 activation leads to DRP-1

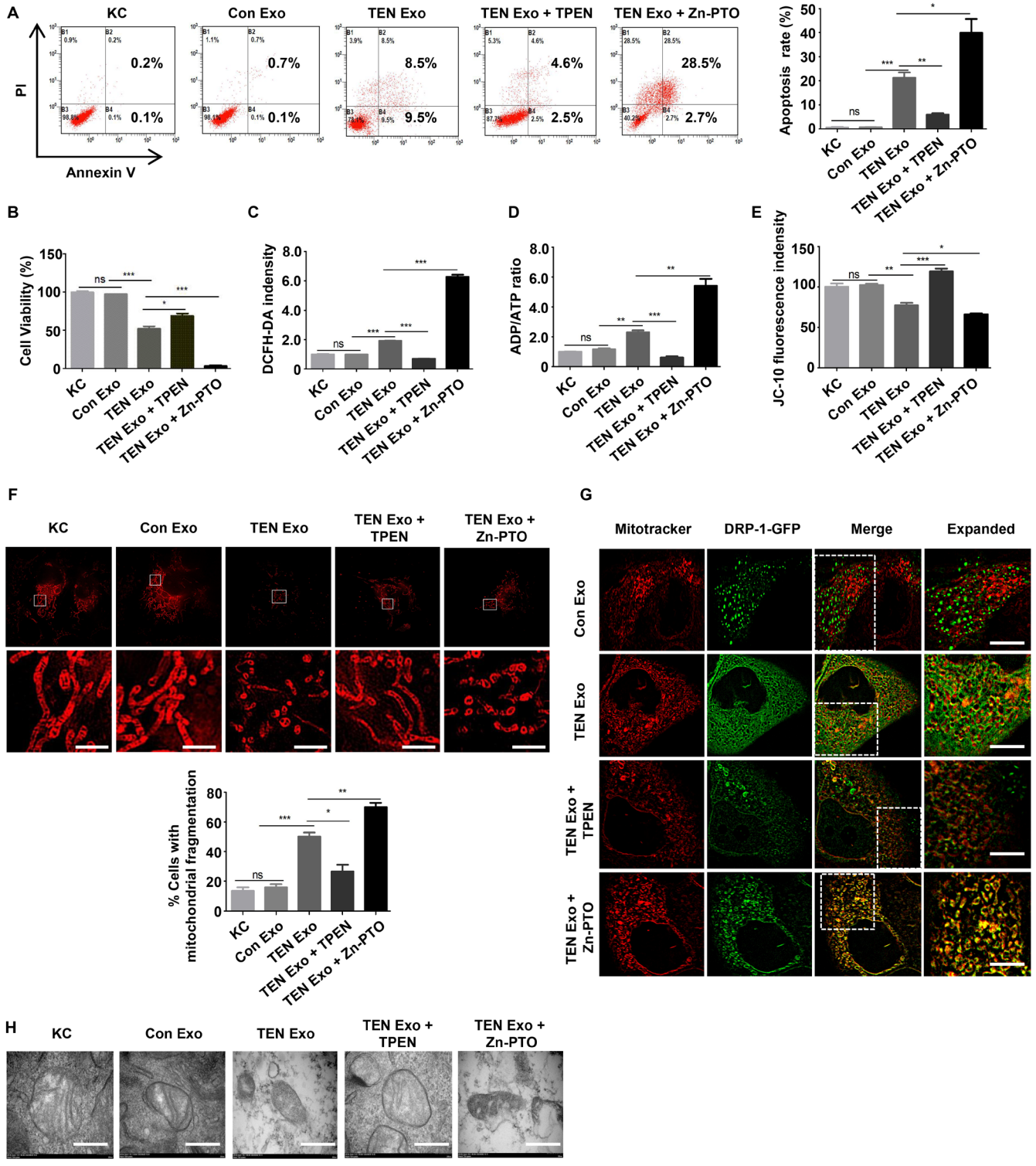

FIGURE 7 | The chelation of Zn^{2+} prevents TEN Exo-induced apoptosis and mitochondrial function and fission in human primary keratinocytes. (A–H) Human primary keratinocytes were treated with BF-derived exosomes obtained by suction surgery in healthy individuals and from TEN patients (100 μg/mL) with or without Zn-PTO (2 μM) or TPEN (3 μM). (A) Apoptosis was determined by fluorescence-activated cell sorting (FACS) analysis with annexin-V/PI staining. (B) CCK-8 assay. (C) The intracellular ROS levels were analyzed by DCFH-DA. (D) ADP/ATP ratio. (E) JC10 assay. (F) HIS-SIM recording of the mitochondrial morphology and cristae of human primary keratinocytes labeled with PKMO. *Bar* = 100 μm. (G) Colocalization of DRP-1 and mitochondria. The boxed area in the right panels represents the amplification of the white square. *Bar* = 200 μm. (H) Representative TEM images of the morphological changes in mitochondria in human primary keratinocytes. *Bar* = 200 μm. The data are reported as the means ± SEMs of three independent experiments. ns, not significant. $^{*}p < 0.05$, $^{**}p < 0.01$, $^{***}p < 0.001$.

recruitment. Our subsequent inquiry focused on the possible contribution of Zn^{2+} to the recruitment of DRP-1. The chelation of Zn^{2+} with TPEN markedly inhibited TEN-Exo-induced DRP-1-GFP recruitment (Figure 7G). Furthermore, the delivery of Zn^{2+} through Zn-PTO stimulated the mitochondrial recruitment of DRP-1-GFP (Figure 7G). The collective results indicate that the galectin-7/TRPM2-mediated elevation of mitochondrial Zn^{2+} concentration promotes DRP-1 recruitment and subsequent mitochondrial fragmentation.

2.10 | DRP-1-Mediated Fission Facilitates HK2 Separation From Mitochondria via the Induction of VDAC1 Oligomerization, Leading to the Opening of the mPTP and Triggering Apoptosis

Increased mitochondrial fission results in prolonged opening of the mPTP and the release of cytochrome c, which ultimately triggers cell apoptosis [21]. Experimental findings demonstrated that interventions such as *DRP-1*-siRNA, mitochondrial division inhibitor-1 (Mdivi-1), and cyclosporine A (CsA)–loaded TEN Exo increased the keratinocyte viability and ATP production while preventing MMP collapse, mitochondrial fission, and apoptosis (Figures S15 and S16). In order to elucidate the mechanism by which fission induces mPTP opening, our first step was to monitor changes in HK2. As illustrated in Figure 8A–C, the treatment of TEN Exo influenced the relocation of HK2 between the mitochondria and cytoplasm, resulting in a decrease in mitochondria-bound HK2 levels and an increase in cytoplasmic HK2. In the magnified image, it is evident that *DRP-1*-siRNA promoted the translocation of HK2 to the mitochondria (Figure 8C). Interestingly, despite the observed reduction in mitochondria-related HK2, there was no alteration in the overall HK2 levels in HaCaT cells following TEN Exo treatment (Figure 8A). This implies that TEN Exo specifically influenced the intracellular distribution of HK2. Due to its direct interaction with VDAC1 to inhibit mPTP opening, we speculated that the dissociation of HK2 from mitochondria was attributed to changes in VDAC1 resulting from DRP-1-mediated fission. Our findings suggested that treatment with TEN Exo significantly reduced the content of VDAC1 but enhanced the formation of VDAC1 oligomers weighing 69 and 95 kDa (Figure 8D). In investigating the impact of VDAC1 oligomerization on HK2 release into the cytoplasm, our focus was on the protein interactions involving HK2 and VDAC1, as well as VDAC1 dimers and multimers. Our results revealed an interaction between VDAC1 and HK2 but not between oligomeric VDAC1 and HK2 (Figure 8E). The findings suggest that DRP-1-mediated fission triggers VDAC1 oligomerization, causing the release of HK2 from the mitochondria. To further substantiate the association between VDAC1 oligomerization, HK2 liberation, and mPTP opening, VBIT-12 and 3-bromopyruvate (3-BrPA) were utilized to inhibit VDAC1 oligomerization and the HK2 interaction, with CsA as the negative control group. The results indicated that blocking the interaction between HK2 and VDAC1 inhibited mPTP opening, whereas the repression of VDAC1 oligomerization increased mPTP opening (Figure 8F). These findings demonstrated that DRP-1-mediated fission facilitates the separation of HK2 from mitochondria via VDAC1 oligomerization, consequently contributing to mPTP opening and keratinocyte apoptosis.

3 | Discussion

It is well known that the basic epidermal pathology in SJS/TEN is large-scale epidermal death, which has been convincingly shown to be the result of keratinocyte apoptosis [2]. Apoptotic cell death can be triggered through extrinsic, granule exocytosis pathways and intrinsic pathways [3]. The extrinsic pathway includes Fas–FasL interactions and TNF-α [3]. The granule exocytosis pathway includes perforin/granzyme and granulysin. The intrinsic pathway is initiated from the mitochondria and can be influenced by Bcl-2 family members [4]. In SJS/TEN, the intrinsic pathway may involve electrophilic toxic drug metabolites produced by keratinocytes [22]. Drug metabolites damage the mitochondria and produce ROS, which directly damages the cellular components [5]. IAPs are a family of proteins that prevent intrinsic apoptosis during cellular stresses. The development of drugs that can inhibit IAPs, such as CompA, provides new opportunities for inducing TEN-like mouse models [7]. Our group has also shown that downregulation of XIAP could promote mitochondrial-dependent apoptosis in SJS/TEN patients [6]. In the present study, impairment of mitochondrial biogenesis was also observed in SJS/TEN lesions, which are considered to constitute a core of mitochondrial dysfunction that subsequently initiates an intrinsic mechanism of apoptosis [23]. Therefore, targeting the mitochondrial-dependent apoptosis pathway may be an attractive therapeutic approach for ameliorating SJS/TEN.

Multiple findings have suggested that large quantities of exosomes are enriched in body fluids [24]. Small extracellular vesicles (sEV) in triple-negative breast cancer (TNBC) patients' plasma could induce mitochondrial stress and initiate relentless intrinsic apoptosis [25]. Recent investigations have revealed that body fluids-derived exosomes promoted mitochondrial dysfunctions and subsequently increased cell apoptosis/necrosis [26]. BF, as a special body fluid in skin diseases, is a valuable biological resource because it provides a means for assessing biomarkers that capture the proteome at the site of skin lesions [12]. BF-derived exosomes contain a mixture of vesicles originating from different sources [13]. Our data showed that a greater number of monocyte-derived $CD14^+/CD63^+$, NK-derived $CD56^+/CD63^+$, and cytotoxic T-cell–derived $CD8^+/CD63^+$ exosomes were present in the TEN-Exo group. Recent studies have revealed that not only T cells and NK cells but also monocytes are involved in the pathogenesis of SJS/TEN [27]. Therefore, we speculated that T cells, NK cells, and monocytes may be the sources of BF-derived exosomes in SJS/TEN patients. However, the potential mechanisms of exosomes secreted into the BF in the context of SJS/TEN remain to be explored.

Exosomal proteins are more stable than regular secretory proteins in body fluids, which makes them perfect candidates as novel biomarkers [28]. In our work, we found that BF-derived exosomes from SJS/TEN patients promoted keratinocyte apoptosis. The determinants of BF-derived exosomes from SJS/TEN patients that trigger keratinocyte pathological change are enriched in apoptosis signaling pathways. Importantly, galectin-7 was the most abundant protein in BF-derived exosomes from SJS/TEN patients. In one study [29], galectin-7 exhibited higher levels in the release of peripheral blood mononuclear cells (PBMCs) from SJS/TEN patients than EM and MPE patients. Disease onset (Day 1) in patients with SJS/TEN was defined as

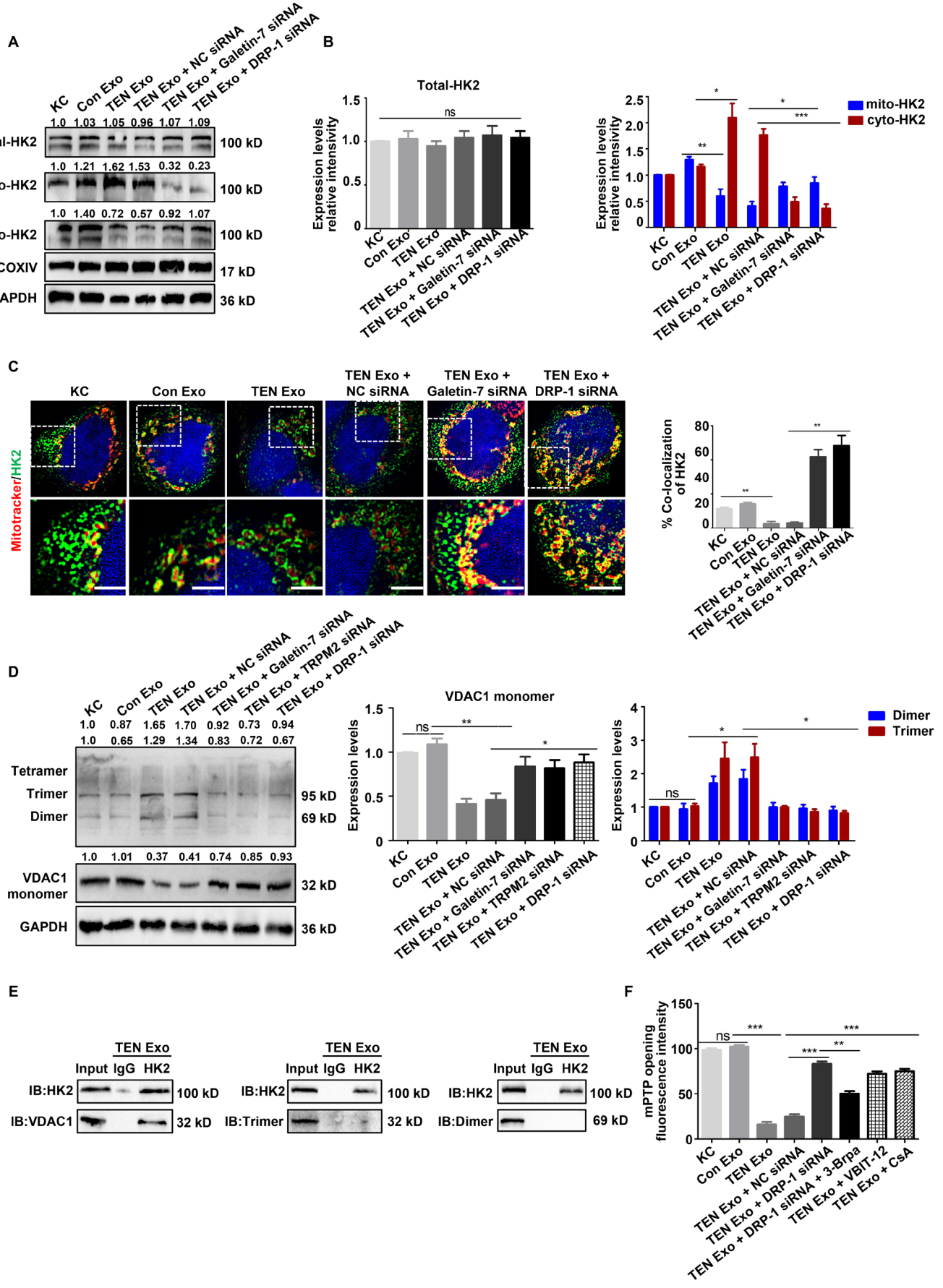

FIGURE 8 | Legend on next page.

FIGURE 8 | DRP-1 axis deficiency inhibits mPTP opening in HaCaT cells via a reduction in VDAC1 oligomerization and subsequent HK2 separation from the mitochondria. (A–C) The subcellular location of HK2 was determined via western blotting and immunofluorescence. Densitometry was used to quantify the expression levels of HK2 relative to those of GAPDH and COXIV. *Bar* = 200 μm. (D) Evaluation of VDAC1 oligomerization via ethylene glycol bis-based cross-linking and immunoblotting using anti-VDAC1 antibodies. (E) HK2 and VDAC1 interactions were assessed by co-IP. (F) mPTP opening by VBIT-12 and 3-Brpa, which are inhibitors of VDAC1 oligomerization and the HK2 interaction, respectively. CsA, an mPTP blocker, was used as the negative control. The data are representative of at least three independent experiments. ns, not significant. $^{*}p < 0.05$, $^{**}p < 0.01$, $^{***}p < 0.001$.

the day when mucocutaneous and/or ocular lesions occurred. Hama et al. [29] collected the serum samples of SJS/TEN before the onset of SJS/TEN. The data showed that serum galectin-7 levels in patients with SJS/TEN at Days −7 to −1 and Days 1 to 7 after onset were significantly higher than those of patients with EM and MPE [29]. In the present study, we concluded that BF or BF-derived exosomes from SJS/TEN patients exhibit increased levels of galectin-7 and that these levels are positively correlated with disease severity. galectin-7 is a keratinocyte-specific marker often found in all layers of the epidermis and is involved in apoptotic responses [30]. Our results also found that galectin-7 was dramatically increased in the epidermis of SJS/TEN skin lesions and was significantly lower after systemic corticosteroids or TNF inhibitor etanercept treatment. Our results further confirm the possible contribution of galectin-7 to the etiology of SJS/TEN. However, the increased levels of galectin-7 were not found in the other keratinocyte death-related blistering diseases such as staphylococcal scalded skin syndrome (SSSS) and bullous systemic lupus erythematosus (BLE). We would conduct a more detailed investigation into whether galectin-7 participated in these diseases in future research. Therefore, galectin-7 may be a specific therapeutic target in SJS/TEN and a promising potential biomarker for diagnosis.

Deciphering the network of galectin-7-interacting proteins is necessary to better understand the key function of galectin-7 in apoptosis initiation. Here, we focused on TRPM2, which we characterized as a novel galectin-7-interacting protein in HaCaT cells. Yamamoto and Shimizu [31] reported that TRPM2 is expressed on the surface of keratinocytes. Our data suggested that the TRPM2 expression levels were significantly upregulated in the epidermis of patients with SJS/TEN. In addition, TRPM2 was diffusely distributed within mitochondria, as indicated by the colocalization of TRPM2 and the mitochondrial marker TOM20 [32]. Our findings clearly highlight the presence of a new galectin-7/TRPM2 complex in mitochondria at a steady state. Interestingly, TRPM2 has been shown to regulate the cell death pathways [31]. Since TRPM2 channels are activated by oxidative stress and correlated with levels of apoptosis [20]. In noncancerous cells, TRPM2 emerges as a viable therapeutic target for conditions such as inflammation, stroke, and diabetes due to the protective effects elicited following TRPM2 antagonism [33–35]. Our study revealed that either *TRPM2* siRNA or an inhibitor could attenuate the apoptotic effects mediated by galectin-7 on keratinocytes. These results suggest that the binding of galectin-7 to TRPM2 may constitute a new target for enhancing keratinocyte apoptosis. Therefore, targeting TRPM2 could be used as a viable strategy to treat SJS/TEN patients in the future. However, the underlying mechanism through which this complex governs apoptosis in SJS/TEN has not been determined.

Mitochondria are highly dynamic organelles whose morphology and constitution are continually changed by fission and fusion processes [8]. During the progression of apoptosis, mitochondrial networks are dramatically reorganized from long filamentous interconnected tubules into small punctate spheres [36]. Because apoptotic cells exhibit a high fission/fusion ratio, fission is believed to be an essential part of the apoptotic process [9]. Recent studies have provided mounting evidence that the inhibition of DRP-1-mediated fission prevents the progression of apoptosis [10], suggesting that mitochondrial fission may also be a driver of apoptosis. In contrast, the knockdown of mitochondrial fusion proteins such as *MFN-2* or *optic atrophy-1* (*OPA-1*) increases susceptibility to apoptosis [37]. Considering the importance of these processes, abnormalities in mitochondrial dynamics and apoptosis occur early during the pathogenesis of diseases such as neurodegenerative diseases and cancer [38]. Here, we demonstrated that the skin lesions of patients with SJS/TEN exhibit reduced MFN-2 expression and increased DRP-1 expression. These results indicate that abnormal mitochondrial dynamics contribute to SJS/TEN pathology.

To gain insight into the underlying mechanism, we first examined the roles of Ca^{2+}, Zn^{2+}, and Mg^{2+} because the intracellular concentrations of these ions are increased by TRPM2 activation [39]. Our results demonstrated that the Zn^{2+} level in mitochondria was higher than that of the other ions in the TRPM2-overexpression group. In addition, the serum Zn^{2+} concentration was significantly higher in SJS/TEN patients than in patients with EM and healthy individuals. To obtain better insight into how Zn^{2+} might affect mitochondrial dynamics, we used TPEN, which chelates Zn^{2+} and is sufficient to prevent mitochondrial fragmentation. This role of Zn^{2+} was further supported by the finding that the delivery of Zn^{2+} through the zinc ionophore Zn-PTO clearly induced mitochondrial fragmentation. Furthermore, TEN Exo induced an increase in mitochondrial Zn^{2+} and the inhibition of TRPM2 channels prevented this increase. In addition, mounting evidence suggests that loss of the MMP, depletion of ATP, and increase in apoptosis are closely associated with mitochondrial fission [40]. Our results indicate that TEN Exo caused a decrease in the MMP and an increase in apoptosis, and these effects were prevented by TPEN pretreatment. Therefore, we conclude that the TRPM2-mediated increase in mitochondrial Zn^{2+} leads to mitochondrial fragmentation, the associated loss of the MMP, and the induction of apoptosis.

To further get mechanistic insight into how TRPM2 signaling regulates mitochondrial fragmentation, we examined the recruitment of DRP-1-GFP to mitochondria. In the present study, we found that TEN Exo increased DRP-1-GFP recruitment to mitochondria, and this recruitment was inhibited by

TRPM2-siRNA. Thus, the galectin-7/TRPM2 complex mediates TEN Exo-induced mitochondrial fission by promoting DRP-1 recruitment to mitochondria. Our data also showed that the chelation of Zn^{2+} with TPEN prevented the recruitment of DRP-1-GFP to mitochondria. In addition, the direct delivery of Zn^{2+} via Zn-PTO induced the recruitment of DRP-1-GFP and mitochondrial fission. These results support a novel role for Zn^{2+} in DRP-1-GFP recruitment and mitochondrial fission.

In mitochondria-mediated cell apoptosis, the opening of the mPTP plays a pivotal role [41]. Recent studies have shown that the association of VDAC1 with HK2 contributes to the inhibition of apoptosis through repression of the formation of the mPTP [42]. Once proapoptotic signals from diverse upstream pathways converge, HK2 dissociates from VDAC1 and subsequently binds to the BCL2 family proapoptotic protein BAX, which alters the mPTP conformation to an open state and results in apoptosis [43]. Our results showed that DRP-1-mediated fission contributes to the dissociation of HK2 from mitochondria, leading to excessive opening of the mPTP, cytochrome c release, and caspase activation. Interestingly, no change in the total expression of HK2 in HaCaT cells was detected after TEN-Exo treatment. Therefore, it is reasonable to hypothesize that the decrease in the content of mitochondrial HK2 is mediated by its low affinity for mitochondria. It has been shown that HK2 binds to VDAC1, which is dynamically oligomerized [44, 45]. We showed that DRP-1-mediated fission can contribute to VDAC1 oligomerization and that VDAC1 oligomers exhibit decreased affinity for HK2, resulting in the separation of HK2 from mitochondria. However, the exact molecular mechanisms by which fission modifies VDAC1 oligomerization remain unclear, and further studies are needed to clarify this point.

The research presented here is subject to certain limitations. One limitation lies in the difficulty of collecting samples at the early disease stage, specifically at the onset of blistering. Owing to the disease's rarity, the difficulty in diagnosing it at an early stage, and its rapid progression, the patients were already in an advanced stage upon admission to the hospital. In order to obtain early-stage samples from SJS/TEN patients, we are currently focusing on collaborating with several dermatology departments to expand our sample collection. We aim to further investigate the dynamics of galectin-7 expression and associated pathway molecules at the early stage of SJS/TEN in the future.

In conclusion, we hypothesized that exosomal galectin-7 enters keratinocytes, combines with TRPM2 in mitochondria, and induces an increase in mitochondrial Zn^{2+}, which leads to enhanced recruitment of the fission factor DRP-1 to mitochondria to trigger excessive mitochondrial fission. The excessive DRP-1-dependent mitochondrial fission via VDAC1/HK2-mediated mPTP opening promoted cytochrome c release and caspase activation, leading to keratinocyte apoptosis in SJS/TEN patients (Figure 9). Upon reviewing these findings, it is evident that targeting galectin-7, TRPM2, and DRP-1 inhibitors may offer innovative therapeutic strategies to impede the progression of epidermal apoptosis in patients with SJS/TEN.

4 | Methods

4.1 | Subjects and Sample Collection

BFs from five SJS patients (two males and three females; average age, 44.8 years) and five TEN patients (five males; average age, 32.6 years) were obtained from the Department of Dermatology in the Xijing Hospital of the Fourth Military Medical University, Shaanxi, China. The clinical characteristics of the SJS/TEN patients are listed in Table S1. This study included BF samples from patients who underwent SJS/TEN, EM, or suction surgery. Suction surgery refers to a suction method to induce a blister in healthy individuals [46, 47]. Serum samples from 12 SJS patients (four males and eight females; average age, 29.73 years) and eight TEN patients (five males and three females; average age, 38.14 years) were also obtained from the Department of Dermatology in the Xijing Hospital. Skin lesions were excised from the skin of three patients who had been pathologically diagnosed with SJS/TEN, EM, MPE, psoriasis, or AD. Skin samples from control subjects were collected from age- and sex-matched healthy individuals undergoing plastic surgery. Besides, all the patients were corticosteroid-naive and were taken at the time of diagnosis. The detailed contents of the institutional review board's ethical approval are shown in Table S2.

4.2 | SP-IRIS Analysis

SP-IRIS is a technology that enhances nanoparticle scatter signals by the application of extra-layered substrates (normally applied silicon oxide). It can detect individual particles captured on an antibody microarray. Briefly, 35 μL of exosomes were diluted in incubation buffer (IB) (1:1) and incubated on ExoView R100 (NanoView Biosciences, Brighton, MA, USA) chips at room temperature for 16 h. Notably, the chips were coated with antibodies against anti-human CD81 (CF 555), CD63 (CF 647), and CD9 (CF 488A). Anti-mouse IgG was used as a negative control. The chips were washed twice with incubation solution, and the plates were shaken at 500 rpm. The chips were then stained with a fluorescent antibody cocktail for 1 h at room temperature in the dark. The fluorophore-conjugated anti-human antibodies used included CD14-FITC, CD8-FITC, CD19-APC, and CD56-APC (eBioscience, San Diego, CA, USA). The chips were washed three times, with a final wash conducted with distilled water, and then imaged using ExoView Scanner 3.1.4 software (NanoView Biosciences).

4.3 | Duolink Proximity Ligation Assay

PLA technology permits detection of protein–protein interactions in situ (at distances < 40 nm) at endogenous protein levels. A proximity ligation assay was performed with a Duolink PLA Kit (#Duo94104; Thermo Fisher) according to the manufacturer's instructions. The HaCaT cells were fixed and incubated overnight with anti-TRPM2 antibody (#166907; Santa Cruz; CA, USA) and antigalectin-7 antibody (#ab10482; Abcam; Cambridge, MA, USA). After multiple washes, the cells were incubated successively with PLA probes, ligation solution, and amplification solution at 37°C. Coverslips were mounted, and

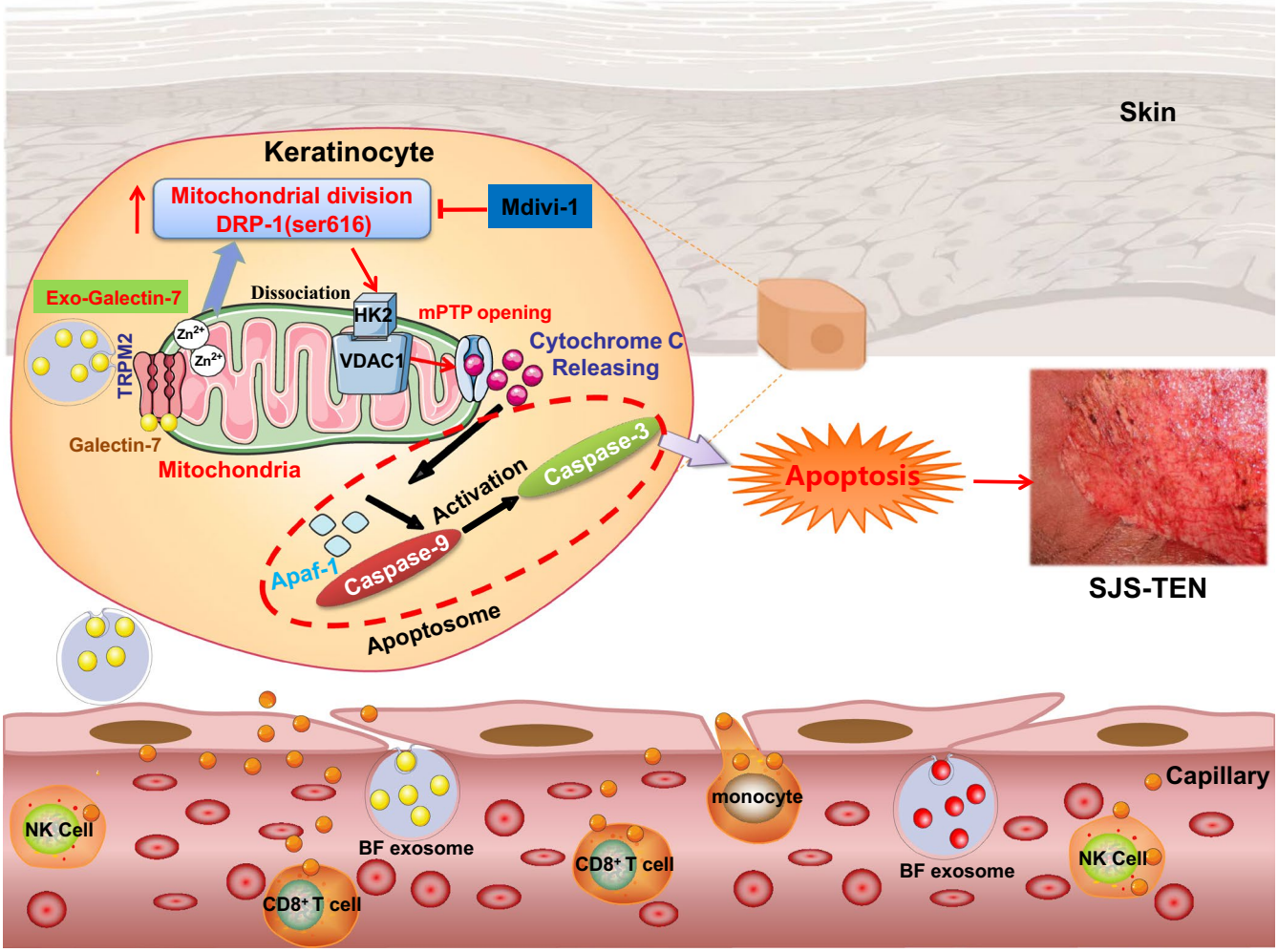

FIGURE 9 | Schematic diagram of the mechanism through which the galectin-7/TRPM2-mediated rise in mitochondrial Zn^{2+} promotes mitochondrial fission and apoptosis in SJS/TEN.

the images were taken using an Olympus FluoView FV1000 confocal microscope.

4.4 | Measurements of the Mitochondrial Cation Levels by ICP–MS

Zinc detection through ionomic analyses was performed with an inductively coupled plasma (ICP)–MS system (Agilent Technologies). ICP–MS can be used to measure elements at trace levels in biological fluids. Quantitative analysis was performed employing the internal standard method, which relies on the intensity ratio of the mass spectrum signal of the target element to be measured and the mass spectrum signal of the internal standard element, directly correlating with the concentration of the target element. Subsequently, ICP–MS analysis was conducted following homogenization.

4.5 | Mitochondrial Fragmentation

After applying the specified treatments, primary human keratinocytes were incubated with DMEM containing 250 nM PKMO for 15 min at 37°C. The cells were then washed once with DMEM, and images were acquired via Hessian–SIM imaging. The Hessian imaging was performed following previously described methods [48].

4.6 | mtDNA Copy Number, Transcription Level Detection, and Respiratory Chain Complex Activity Assays

The relative mtDNA copy number was measured by RT-PCR as previously described [49]. The ratio of the mitochondrial NADH dehydrogenase 1 (MT-ND1) gene in mtDNA to the single copy nuclear gene human globulin (HGB) was determined from standard curves.

The transcript level of mtDNA is indicated by two distinct components: ND1 encoded by the light chain of mtDNA, and cytochrome c oxidase subunit I derived from the heavy chain.

The mitochondrial complex I, III, and IV reagents were purchased from Solarbio (Beijing, China), and the activities were assessed following the manufacturer's instructions. The primers used are listed in Table S5.

4.7 | Loading Plasmids and siRNAs Into Exosomes

Briefly, 50 μg of exosomes isolated from human BF of SJS/TEN patients were incubated with Exo-Fect siRNA transfection kit reagent (EXFT20A; System Biosciences, CA, USA) and with *Galectin-7, TRPM2, S100A9, PDCD6*, and *DRP-1* siRNA (10 pM) or galectin-7, TRPM2, DRP-1, or DRP-1-GFP plasmids (1 μg) at 37°C for 10 min, placed on ice for 30 min, washed three times with PBS, and centrifuged at 2000 *g* and 4°C for 30 min [50–52]. The cells transfected with exosomes were used in the subsequent experiments.

4.8 | Statistical Analysis

The data were subjected to the Mann–Whitney *U* test and one-way ANOVA to compare group means, which were conducted with GraphPad Prism software version 6 (GraphPad software). Prior to conducting parametric tests, normality of the data was checked. Evaluation of Pearson's correlation coefficients was conducted, with a significance level set at $p < 0.05$. The significance level (p value) for Pearson's correlation coefficient (R) was obtained by a t-test formula: $t = \frac{R}{\sqrt{\frac{1-R^2}{n-2}}}$ with degrees of freedom (df) = $n-2$. Data are reported as means ± SEMs based on triplicate values obtained from three experiments.

Author Contributions

C.Z., B.Y.P., Y.X.L., Z.C., and P.Q. performed the experiments and processed the samples; H.F., Q.J., and E.L.D. conducted the clinical investigations; Z.L.Z., J.K.Y., P.K., A.H., and S.X.S. performed the bioinformatics analyses; and R.A., H.J.Q., G.W., and M.F. designed the study and wrote the manuscript.

Acknowledgments

We thank Professor GuoDong Yang and Rui Zhang for their helpful suggestions for this manuscript. We thank the Analysis & Testing Laboratory for Life Sciences and Medicine of Fourth Military Medical University for live imaging. We thank Guangzhou CSR Biotech Co. Ltd. for the live-cell imaging via commercial superresolution microscopy (HIS-SIM), data acquisition, and SR image reconstruction, analysis, and discussion. We also thank Yufei Wang and Ning Li (Quantum Design China & NanoView Biosciences) for supporting the characterization of extracellular vesicles.

Ethics Statement

Human subject was approved by the Ethics Committee of the First Affiliated Hospital of Fourth Military Medical University (IRB number: KY20172030-1).

Conflicts of Interest

The authors declare no conflicts of interest.

Data Availability Statement

The data that support the findings of this study are available from the corresponding authors upon reasonable request. Values for all data points in graphs are reported in the Data S2. The proteomics data have been deposited in the ProteomeXchange Consortium (https://proteomecentral.proteomexchange.org) via the iProX partner repository with the dataset identifier PXD059206.

References

1. A. Gibson, P. Deshpande, C. N. Campbell, et al., "Updates on the Immunopathology and Genomics of Severe Cutaneous Adverse Drug Reactions," *Journal of Allergy and Clinical Immunology* 151, no. 2 (2023): 289–300.

2. A. Hasegawa and R. Abe, "Recent Advances in Managing and Understanding Stevens-Johnson Syndrome and Toxic Epidermal Necrolysis," *F1000Research* 16, no. 9 (2020): 612.

3. J. Y. Yuan and D. Ofengeim, "A Guide to Cell Death Pathways," *Nature Reviews. Molecular Cell Biology* 25, no. 5 (2024): 379–395.

4. Y. Ai, Y. Meng, B. Yan, Q. Zhou, and X. Wang, "The Biochemical Pathways of Apoptotic, Necroptotic, Pyroptotic, and Ferroptotic Cell Death," *Molecular Cell* 84, no. 1 (2024): 170–179.

5. P. Paquet and G. E. Pierard, "Toxic Epidermal Necrolysis: Revisiting the Tentative Link Between Early Apoptosis and Late Necrosis," *International Journal of Molecular Medicine* 19, no. 1 (2007): 3–10.

6. C. Zhang, Z. L. Zhu, J. X. Gao, et al., "Plasma Exosomal miR-375-3p Regulates Mitochondria-Dependent Keratinocyte Apoptosis by Targeting XIAP in Severe Drug-Induced Skin Reactions," *Science Translational Medicine* 12, no. 574 (2020): eaaw6142.

7. T. M. Nordmann, H. Anderton, A. Hasegawa, et al., "Spatial Proteomics Identifies JAKi as Treatment for a Lethal Skin Disease," *Nature* 635, no. 8040 (2024): 1001–1009.

8. R. Quintana-Cabrera and L. Scorrano, "Determinants and Outcomes of Mitochondrial Dynamics," *Molecular Cell* 83, no. 6 (2023): 857–876.

9. R. J. Youle and A. M. van der Bliek, "Mitochondrial Fission, Fusion, and Stress," *Science* 337, no. 6098 (2012): 1062–1065.

10. M. Karbowski, Y. J. Lee, B. Gaume, et al., "Spatial and Temporal Association of Bax With Mitochondrial Fission Sites, Drp1, and Mfn2 During Apoptosis," *Journal of Cell Biology* 159, no. 6 (2002): 931–938.

11. A. Kaasik, D. Safiulina, A. Zharkovsky, and V. Veksler, "Regulation of Mitochondrial Matrix Volume," *American Journal of Physiology. Cell Physiology* 292, no. 1 (2007): C157–C163.

12. A. Gibson, R. Ram, R. Gangula, et al., "Multiomic Single-Cell Sequencing Defines Tissue-Specific Responses in Stevens-Johnson Syndrome and Toxic Epidermal Necrolysis," *Nature Communications* 15, no. 1 (2024): 8722.

13. H. Fang, S. Shao, M. Jiang, et al., "Proinflammatory Role of Blister Fluid-Derived Exosomes in Bullous Pemphigoid," *Journal of Pathology* 245, no. 1 (2018): 114–125.

14. B. Purghè, M. Manfredi, B. Ragnoli, G. Baldanzi, and M. Malerba, "Exosomes in Chronic Respiratory Diseases," *Biomedicine & Pharmacotherapy* 144 (2021): 112270.

15. B. N. Whitley, E. A. Engelhart, and S. Hoppins, "Mitochondrial Dynamics and Their Potential as a Therapeutic Target," *Mitochondrion* 49 (2019): 269–283.

16. S. Cogliati, C. Frezza, M. E. Soriano, et al., "Mitochondrial Cristae Shape Determines Respiratory Chain Supercomplexes Assembly and Respiratory Efficiency," *Cell* 155, no. 1 (2013): 160–171.

17. P. T. Manna, T. S. Munsey, N. Abuarab, et al., "TRPM2 Mediated Intracellular Zn^{2+} Release Triggers Pancreatic beta Cell Death," *Biochemical Journal* 466, no. 3 (2015): 537–546.

18. L. M. Malaiyandi, O. Vergun, K. E. Dineley, and I. J. Reynolds, "Direct Visualization of Mitochondrial Zinc Accumulation Reveals Uniporter-Dependent and -Independent Transport Mechanisms," *Journal of Neurochemistry* 93, no. 5 (2005): 1242–1250.

19. H. Tian and Z. Y. Wang, "Zinc chelator Inhibits Zinc-Induced Islet Amyloid Polypeptide Deposition and Apoptosis in INS-1 Cells," *Biological Trace Element Research* 189, no. 1 (2019): 201–208.

20. N. Abuarab, T. S. Munsey, L. H. Jiang, et al., "High Glucose Induced ROS Activates TRPM2 to Trigger Lysosomal Membrane Permeabilization and Zn^{2+}-Mediated Mitochondrial Fission," *Science Signaling* 10, no. 490 (2017): eaal4161.

21. X. Chang, A. Lochner, H. H. Wang, et al., "Coronary Microvascular Injury in Myocardial Infarction: Perception and Knowledge for Mitochondrial Quality Control," *Theranostics* 11, no. 14 (2021): 6766–6785.

22. N. Singh and M. Phillips, "Toxic Epidermal Necrolysis: A Review of Past and Present Therapeutic Approaches," *Skin Therapy Letter* 27, no. 5 (2022): 7–13.

23. V. Sorrentino, K. J. Menzies, and J. Auwerx, "Repairing Mitochondrial Dysfunction in Disease," *Annual Review of Pharmacology and Toxicology* 58 (2018): 353–389.

24. D. Yu, Y. X. Li, M. Y. Wang, et al., "Exosomes as a New Frontier of cancer Liquid Biopsy," *Molecular Cancer* 21, no. 1 (2022): 56.

25. S. K. Mondal, D. Haas, J. Han, and T. L. Whiteside, "Small EV in Plasma of Triple Negative Breast Cancer Patients Induce Intrinsic Apoptosis in Activated T Cells," *Communications Biology* 6, no. 1 (2023): 815.

26. C. Y. Tsai, S. C. Hsieh, C. S. Lu, et al., "Cross-Talk Between Mitochondrial Dysfunction-Provoked: Oxidative Stress and Aberrant Noncoding RNA Expression in the Pathogenesis and Pathophysiology of SLE," *International Journal of Molecular Sciences* 20, no. 20 (2019): 5183.

27. Y. Saito and R. Abe, "New Insights Into the Diagnosis and Management of Stevens-Johnson Syndrome and Toxic Epidermal Necrolysis," *Current Opinion in Allergy and Clinical Immunology* 23, no. 4 (2023): 271–278.

28. A. C. Müller, F. P. Breitwieser, H. Fischer, et al., "A Comparative Proteomic Study of Human Skin Suction Blister Fluid From Healthy Individuals Using Immunodepletion and iTRAQ Labeling," *Journal of Proteome Research* 11, no. 7 (2012): 3715–3727.

29. N. Hama, K. Nishimura, A. Hasegawa, et al., "Galectin-7 as a Potential Biomarker of Stevens-Johnson Syndrome/Toxic Epidermal Necrolysis: Identification by Targeted Proteomics Using Causative Drug-Exposed Peripheral Blood Cells," *Journal of Allergy and Clinical Immunology: In Practice* 7, no. 8 (2019): 2894–2897.

30. C. Villeneuve, L. Baricault, L. Canelle, et al., "Mitochondrial Proteomic Approach Reveals Galectin-7 as a Novel BCL-2 Binding Protein in Human Cells," *Molecular Biology of the Cell* 22, no. 7 (2011): 999–1013.

31. S. Yamamoto and S. Shimizu, "Targeting TRPM2 in ROS-Coupled Diseases," *Pharmaceuticals* 9, no. 3 (2016): 57.

32. B. F. Yu, L. N. Jin, X. Yao, et al., "TRPM2 Protects Against Cisplatin-Induced Acute Kidney Injury and Mitochondrial Dysfunction via Modulating Autophagy," *Theranostics* 13, no. 13 (2023): 4356–4375.

33. K. Takahashi, K. Sakamoto, and J. Kimura, "Hypoxic Stress Induces Transient Receptor Potential Melastatin 2 (TRPM2) Channel Expression in Adult Rat Cardiac Fibroblasts," *Journal of Pharmacological Sciences* 118, no. 2 (2012): 186–197.

34. E. Fonfria, I. C. Marshall, I. Boyfield, et al., "Amyloid Beta-Peptide(1-42) and Hydrogen Peroxide-Induced Toxicity Are Mediated by TRPM2 in Rat Primary Striatal Cultures," *Journal of Neurochemistry* 95, no. 3 (2005): 715–723.

35. I. Lange, S. Yamamoto, S. Partida-Sanchez, Y. Mori, A. Fleig, and R. Penner, "TRPM2 Functions as a Lysosomal Ca^{2+}-Release Channel in Beta Cells," *Science Signaling* 2, no. 71 (2009): ra23.

36. C. Sheridan and S. J. Martin, "Mitochondrial Fission/Fusion Dynamics and Apoptosis," *Mitochondrion* 10, no. 6 (2010): 640–648.

37. W. Chen, H. Zhao, and Y. Li, "Mitochondrial Dynamics in Health and Disease: Mechanisms and Potential Targets," *Signal Transduction and Targeted Therapy* 8, no. 1 (2023): 333.

38. D. C. Chan, "Mitochondrial Dynamics and Its Involvement in Disease," *Annual Review of Pathology* 24 (2020): 235–259.

39. F. Li, T. S. Munsey, and A. Sivaprasadarao, "TRPM2-Mediated Rise in Mitochondrial Zn^{2+} Promotes Palmitate-Induced Mitochondrial Fission and Pancreatic β-Cell Death in Rodents," *Cell Death and Differentiation* 24, no. 12 (2017): 1999–2012.

40. K. E. Dineley, L. L. Richards, T. V. Votyakova, and I. J. Reynolds, "Zinc Causes Loss of Membrane Potential and Elevates Reactive Oxygen Species in Rat Brain Mitochondria," *Mitochondrion* 5, no. 1 (2005): 55–65.

41. E. Jacotot, P. Costantini, E. Laboureau, et al., "Mitochondrial Membrane Permeabilization During the Apoptotic Process," *Annals of the New York Academy of Sciences* 887 (1999): 18–30.

42. D. W. Zhang, Y. M. Yip, and L. B. Li, "In Silico Construction of HK2-VDAC1 Complex and Investigating the HK2 Binding-Induced Molecular Gating Mechanism of VDAC1," *Mitochondrion* 30 (2016): 222–228.

43. R. Zalk, A. Israelson, E. S. Garty, et al., "Oligomeric States of the Voltage-Dependent Anion Channel and Cytochrome c Release From Mitochondria," *Biochemical Journal* 386 (2005): 73–83.

44. Y. Li, J. Kang, J. Fu, et al., "PGC1α Promotes Cisplatin Resistance in Ovarian Cancer by Regulating the HSP70/HK2/VDAC1 Signaling Pathway," *International Journal of Molecular Sciences* 22, no. 5 (2021): 2537.

45. H. Zhou, Y. Zhang, S. Hu, et al., "Melatonin Protects Cardiac Microvasculature Against Ischemia/Reperfusion Injury via Suppression of Mitochondrial Fission-VDAC1-HK2-mPTP-Mitophagy axis," *Journal of Pineal Research* 63, no. 1 (2017): e12413.

46. F. J. P. M. Huygen, N. Ramdhani, A. V. Toorenenbergen, et al., "Mast Cells Are Involved in Inflammatory Reactions During Complex Regional Pain Syndrome Type 1," *Immunology Letters* 91, no. 2–3 (2004): 147–154.

47. F. J. P. M. Huygen, A. G. J. D. Bruijn, M. T. D. Bruin, et al., "Evidence for Local Inflammation in Complex Regional Pain Syndrome Type 1," *Mediators of Inflammation* 11, no. 1 (2002): 47–51.

48. W. Zhao, S. Zhao, L. Li, et al., "Sparse Deconvolution Improves the Resolution of Live-Cell Super-Resolution Fluorescence Microscopy," *Nature Biotechnology* 40, no. 4 (2022): 606–617.

49. J. L. Xing, M. Chen, C. G. Wood, et al., "Mitochondrial DNA Content: Its Genetic Heritability and Association With Renal Cell Carcinoma," *Journal of the National Cancer Institute* 100, no. 15 (2008): 1104–1112.

50. Z. Chen, H. Q. Wang, Y. Xia, F. Yan, and Y. Lu, "Therapeutic Potential of Mesenchymal Cell-Derived miRNA-150-5p-Expressing Exosomes in Rheumatoid Arthritis Mediated by the Modulation of MMP14 and VEGF," *Journal of Immunology* 201, no. 8 (2018): 2472–2482.

51. D. M. Pegtel, K. Cosmopoulos, D. A. Thorley-Lawson, et al., "Functional Delivery of Viral miRNAs via Exosomes," *Proceedings of the National Academy of Sciences of the United States of America* 107, no. 14 (2010): 6328–6333.

52. L. A. Erviti, Y. Q. Seow, H. F. Yin, et al., "Delivery of siRNA to the Mouse Brain by Systemic Injection of Targeted Exosomes," *Nature Biotechnology* 29, no. 4 (2011): 341–345.

Supporting Information

Additional supporting information can be found online in the Supporting Information section.